# Grain Refinement of Pure Al using $Al_{2.5}Cu_{0.5}Ti$ Particles with an $L1_2$ Structure

Yoshimi Watanabe *, Ryosuke Yamazaki, Kunika Yamanaka and Hisashi Sato
Nagoya Institute of Technology, Gokiso-cho, Showa-ku, Nagoya 466-8555, Japan
Email of corresponding author: yoshimi@nitech.ac.jp

~~In this study,~~ an $L1_2$-modified $Al_{2.5}Cu_{0.5}Ti$ intermetallic compound was chosen as a heterogeneous nucleation site to develop grain refiners for cast Al with a high volume fraction of heterogeneous nucleation site particles. $Al_{2.5}Cu_{0.5}Ti$ intermetallic compound particles with an $L1_2$ structure were prepared by crushing the bulk material obtained by arc melting or directly by gas atomization. Al-10 vol% $Al_{2.5}Cu_{0.5}Ti$, Al-20 vol% $Al_{2.5}Cu_{0.5}Ti$, Al-30 vol% $Al_{2.5}Cu_{0.5}Ti$ and Al-40 vol% $Al_{2.5}Cu_{0.5}Ti$ refiners were fabricated by the spark plasma sintering method. The grain refining performance of the fabricated refiners for pure cast Al was investigated. ~~It was found that~~ fabricated Al-$Al_{2.5}Cu_{0.5}Ti$ refiners were effective grain refiners for cast Al because $Al_{2.5}Cu_{0.5}Ti$ particles with the $L1_2$ structure acts as nuclei for Al grains in Al melts. Different refining performance characteristics appeared for refiners with different volume fraction of heterogeneous nucleation site particles, even though the total amount of particles in the melt was the same. ~~Moreover,~~ superior grain refining efficiency was obtained for the $Al_{2.5}Cu_{0.5}Ti$ particles having a single phase than those with secondary phase. This is because the lattice matching between heterogeneous nucleation site particles and solidified Al is critical to obtain finer grain structures for Al casts.

Key words
Cast Al, Grain refiner, Heterogeneous nucleation site, $L1_2$ structure, Spark plasma sintering (SPS)

* Corresponding author: Prof. Yoshimi Watanabe, Department of Physical Science and Engineering, Graduate School of Engineering, Nagoya Institute of Technology, Gokiso-cho, Showa-ku, Nagoya 466-8555, Japan, Tel.: +81-52-735-5624, e-mail: yoshimi@nitech.ac.jp

## 1. Introduction

The most widely used refiner for Al cast alloys is the Al-5 mass% Ti-1 mass% B alloy (Fan et al., 2015), in which $Al_3Ti$ intermetallic compound particles and $TiB_2$ particles act as heterogeneous nucleation sites. There are two approaches to enhance the refining performance of grain refiners. One is a very simple method, which can be achieved by increasing the number of heterogeneous nucleation sites in the melt. For example, the effect of hot-rolling Al-5 mass% Ti-1 mass% B refiner on the grain refining efficiency for Al cast was studied by Venkateswarlu et al. (2001). It is reported that hot-rolling, which causes the fracture of $Al_3Ti$ particles, improves the grain refining efficiency of the refiner. The grain refining performance of severely plastic deformed Al-5 mass% Ti-0.25 mass% C refiner was investigated by Zhang et al. (2005a), where better refining performance was reported for severely plastic deformed Al-5 mass% Ti and Al-5 mass% Ti–0.25 mass% C refiner due to a decrease in the mean size of TiC particles and an increase in the number of potent TiC nucleus particles in the refiner (Zhang et al., 2005a). The effects of cold-rolling for Al-5 mass% Ti refiner on the grain refinement of as-cast pure Al were investigated by Sato et al. (2013). The grain size of the α-Al grains was found to decrease as the ratio of refiners was reduced due to an increase in the number of $Al_3Ti$ particles and heterogeneous nucleation sites in the refiner. An increase in the number of heterogeneous nucleation sites in the melt could also be accomplished using a refiner with a high volume fraction of heterogeneous nucleation site particles, whereby the amount of refiner required could be reduced. One of the aims of this study is the development of refiners with a high volume fraction of heterogeneous nucleation site particles.

The second approach is an improvement of the lattice matching between heterogeneous nucleation sites and the nucleating phase. The degree of effectiveness of the heterogeneous nucleation is explained based on the disregistry between the lattice parameters of the heterogeneous nucleation sites and the nucleating phase. Turnbull and Vonnegut (1952) proposed the following equation to evaluate this disregistry:

$$\delta = \frac{|a_s - a_n|}{a_n} \times 100\%, \qquad (1)$$

where $a_s$ and $a_n$ are the lattice parameters of the heterogeneous nucleation sites and the nucleating phase without deformation, respectively. However, the $Al_3Ti$ phase has the tetragonal $D0_{22}$ structure; therefore, the atomic arrangement does not have exact

symmetry. Alternatively, the planar disregistry proposed by Bramfitt (1970) is given by:

$$\delta_{(hkl)_n}^{(hkl)_s} = \frac{1}{3}\sum_{i=1}^{3}\left\{\left|d[uvw]_s^i \cos\theta - d[uvw]_n^i\right| \Big/ d[uvw]_n^i\right\} \times 100\%, \qquad (2)$$

and this is often used (Honda et al., 2008), where $(hkl)_s$ and $(hkl)_n$ are the low-index planes of the heterogeneous nucleation sites and nucleating phase, respectively, $[uvw]_s$ and $[uvw]_n$ are the low-index orientations on $(hkl)_s$ and $(hkl)_n$, respectively, $d[uvw]_s$ and $d[uvw]_n$ are the interatomic spacing distances along $[uvw]$, and $\theta$ is the angle between $[uvw]_s$ and $[uvw]_n$. However, the physical meaning of the plane disregistry is not clear, for example, why three in-plane directions are considered to evaluate planar disregistry (Watanabe et al. 2017a). On the other hand, Kato et al. (1989) have investigated the preferred epitaxial relationship (crystallographic orientation relationship) between a deposit and substrate of metals using the parameter *M,* where the parameter *M* is defined as:

$$M = \varepsilon_1^2 + \varepsilon_2^2 + (2/3)\,\varepsilon_1\,\varepsilon_2, \qquad (3)$$

where $\varepsilon_1$ and $\varepsilon_2$ are the principal misfit strains calculated from the principal distortions. According to their study, the epitaxial relationship with smaller *M* value becomes the preferred relationship. Although this consideration has been often applied for epitaxial phenomena, it is potentially applicable to predict the effective nucleant materials. Based on the unit cell structures of Al and $Al_3Ti$ shown in Fig. 1, *M* values for low-index planes were calculated using the lattice parameters $a = 0.4049$ nm for Al, and $a = 0.3851$ nm and $c = 0.8608$ nm for $Al_3Ti$, and the results are listed in Table 1. The lattice parameters of $a = 0.3038$ nm and $c = 0.32392$ nm for $TiB_2$ are used, because Zhang et al. (2005b) used these values to predict the effectiveness of heterogeneous nucleation sites for Al alloy. $Al_3Ti$ in Al-Ti alloy is known to be platelet shaped (Watanabe et al. 2001). Yamashita et al. (2000) reported that the *c* axis of $Al_3Ti$, $[001]_{Al3Ti}$, is almost perpendicular to the wide plane of the platelet. Therefore, the dominant face of $Al_3Ti$ platelets is not the best plane for heterogeneous nucleation, because it has the largest *M* value among the above orientation relationships (Watanabe et al. 2017a), as shown in Table 1. On the other hand, $Al_3Ti$ with the $D0_{22}$ type tetragonal structure can undergo a phase transformation to the high-symmetry $L1_2$ cubic structure by the addition of elements from the third period of the periodic table (Inoue et al. 1991). Nakayama and Mabuchi (1993) have reported that $L1_2$ modified $(Al_{1-x}Me_x)_3Ti$ intermetallic compounds (*Me*= Cr, Mn, Fe, Co, Ni, Cu, Zn,

Rh, Pd, Ag, Pt and Au) could be fabricated by sintering of elemental powders. The microstructure of laser-processed $(Al_{1-x}Ni_x)_3Ti$ has been studied by GunnÆs et al. (1998). Figure 1 shows the Al-rich corner of the Al-*Me*-Ti (*Me* = Ni, Fe and Cu) alloy diagram at 1200 °C, after Mazdiyasni et al. (1989). Schematic illustrations of $Al_3Ti$ with the $D0_{22}$ structure, Al with an fcc structure and $(Al_{1-x}Me_x)_3Ti$ with the $L1_2$ structure, as well as their lattice parameters, after Villars and Calvert (1996), are also shown in this figure. The oval-shaped regions represent the extent of the $L1_2$ structure fields in the Ni, Fe, and Cu systems at 1200 °C, and they lie along the straight line with 25 mol% Ti, and have compositions of $Al_{2.68}Ni_{0.32}Ti$, $Al_{2.75}Fe_{0.375}Ti$ and $Al_{2.5}Cu_{0.5}Ti$, respectively (Mabuchi and Nakayama, 1991).

Table 1. *M* values between Al and $Al_3Ti$, $TiB_2$ or $Al_{2.5}Cu_{0.5}Ti$.

| Interface | *M* [x$10^{-3}$] |
|---|---|
| $(100)_{Al}$ // $(100)_{Al_3Ti}$ | 4.31 |
| $(001)_{Al}$ // $(001)_{Al_3Ti}$ | 6.38 |
| $(110)_{Al}$ // $(110)_{Al_3Ti}$ | 4.31 |
| $(111)_{Al}$ // $(112)_{Al_3Ti}$ | 2.24 |
| $(110)_{Al}$ // $(001)_{Al_3Ti}$ | 2.18 |
| $(111)_{Al}$ // $(0001)_{TiB_2}$ | 9.95 |
| $(hkl)_{Al}$ // $(hkl)_{Al_{2.5}Cu_{0.5}Ti}$ | 2.57 |

Among these, the $Al_{2.5}Cu_{0.5}Ti$ intermetallic compound has a wide $L1_2$ structure region in the ternary phase diagram. The lattice constant of the $Al_{2.5}Cu_{0.5}Ti$ intermetallic compound with the $L1_2$ structure is $a = 0.3927$ nm (Villars and Calvert (1996)); therefore, better lattice matching between the heterogeneous nucleation sites and the nucleating phase can be achieved, as shown in Table 1. However, the $Al_{2.5}Cu_{0.5}Ti$ intermetallic compound cannot coexist with an Al matrix in equilibrium. This problem could be overcome by the use of the spark plasma sintering (SPS) method, which is a recently developed consolidation method that allows the compacted powders to be sintered at a low temperature with short heating, holding and cooling times (Zhang et al. 2013). Watanabe et al. (2016 and 2017b) have successfully fabricated an Al–$L1_2$-type $Al_{2.7}Fe_{0.3}Ti$ refiner using the SPS method.

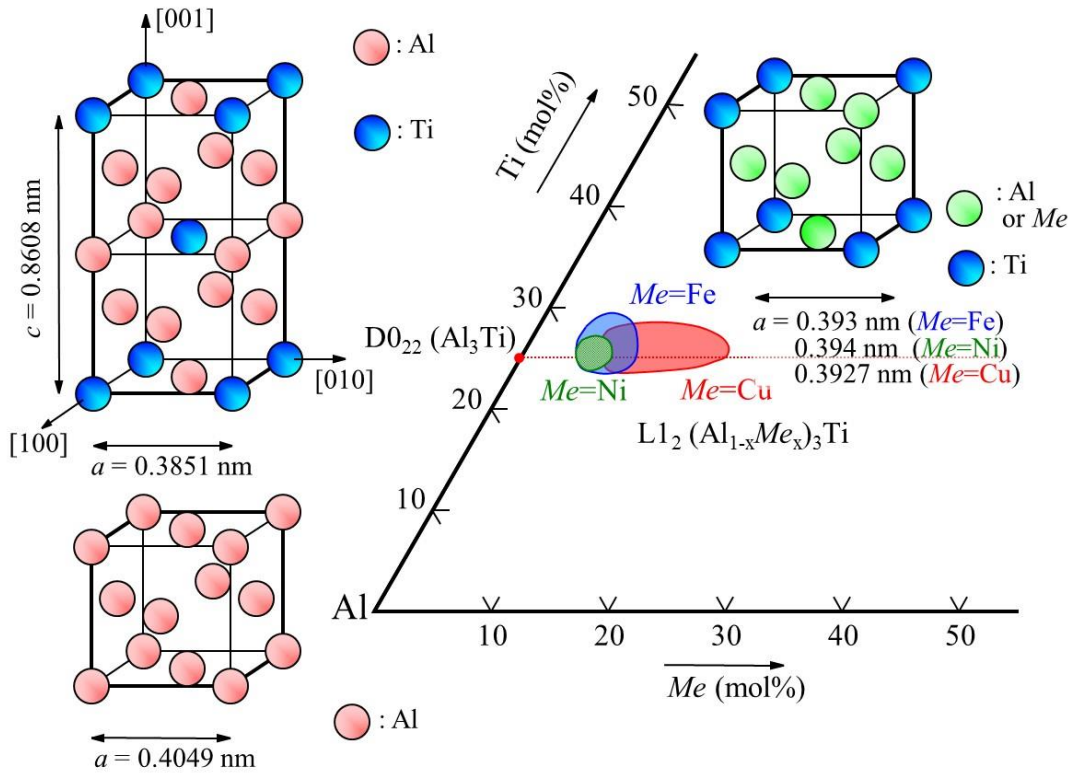


Fig. 1. Al-rich corner of the Al-*Me*-Ti (*Me* = Ni, Fe and Cu) alloy diagram at 1200 °C showing $L1_2$ regions, after Mazdiyasni et al. (1989). Schematic illustrations of $Al_3Ti$ with the $D0_{22}$ structure, Al with an fcc structure and $(Al_{1-x}Me_x)_3Ti$ with the $L1_2$ structure, as well as their lattice parameters, after Villars and Calvert (1996).

Considering these results, $Al_{2.5}Cu_{0.5}Ti$ intermetallic compound with the $L1_2$ cubic structure was selected for the heterogeneous nucleation sites in this study. Al-$Al_{2.5}Cu_{0.5}Ti$ refiners with a high volume fraction of $Al_{2.5}Cu_{0.5}Ti$ particles were investigated. First, $Al_{2.5}Cu_{0.5}Ti$ intermetallic compound particles with the $L1_2$ structure were prepared by crushing of the bulk material obtained by arc melting or directly by gas atomization. Al-10 vol% $Al_{2.5}Cu_{0.5}Ti$, Al-20 vol% $Al_{2.5}Cu_{0.5}Ti$, Al-30 vol% $Al_{2.5}Cu_{0.5}Ti$ and Al-40 vol% $Al_{2.5}Cu_{0.5}Ti$ refiners were then fabricated by the SPS method. The grain refining performance of the fabricated refiners for pure Al cast was thus investigated.

## 2. Experimental Procedure

### 2.1 Fabrication of Al- $Al_{2.5}Cu_{0.5}Ti$ refiners

Figure 2 shows a flow diagram for the fabrication process of novel Al-$Al_{2.5}Cu_{0.5}Ti$ refiners. In this study, two types of $Al_{2.5}Cu_{0.5}Ti$ intermetallic compound

particles with the $L1_2$ structure were used. One was prepared by the gas atomization method, which has potential for mass production. Hereafter, the particles prepared by the gas atomization method will be denoted as “atomized particles”. The atomization gas pressure, orifice diameter, differential pressure and holding temperature of molten metal were 4.5 MPa, 2.2 mm, 40 kPa, and 1550 °C, respectively.

The other type of $Al_{2.5}Cu_{0.5}Ti$ intermetallic compound particles were “crushed particles”. The $Al_{2.5}Cu_{0.5}Ti$ intermetallic compound with the $L1_2$ structure was first prepared by arc melting of pure Al (99.7%), pure Ti (99.9%) and Al-40 mass% Cu alloy under an argon atmosphere. Homogenization of the samples was then performed at 1100 °C for 4 h in an evacuated quartz capsule. The $L1_2$-modified $Al_3Ti$ has been reported to remain brittle under tension and exhibits a fracture mode of brittle transgranular type cleavage (George et al. 1990). The $Al_{2.5}Cu_{0.5}Ti$ intermetallic compound can therefore be crushed into fine particles with a hammer.

Both atomized particles and crushed particles were sieved into a size range of 75–150 μm, and were mixed with pure Al particles (99.9%, 180–425 μm). The volume fractions of intermetallic compound particles were 10, 20, 30, and 40 vol%. Sintering of the mixed-powders with the SPS apparatus (SPS-515S, SPS Syntax Inc.) was performed at 500 °C for 5 min under an applied stress of 45 MPa. The Al-10 vol% $Al_{2.5}Cu_{0.5}Ti$, Al-20 vol% $Al_{2.5}Cu_{0.5}Ti$, Al-30 vol% $Al_{2.5}Cu_{0.5}Ti$, and Al-40 vol% $Al_{2.5}Cu_{0.5}Ti$ refiners containing atomized particles are denoted as 10 vol%, 20 vol%, 30 vol%, and 40 vol% atomization refiners, respectively. The Al-10 vol% $Al_{2.5}Cu_{0.5}Ti$ refiner and Al-20 vol% $Al_{2.5}Cu_{0.5}Ti$ refiner containing crushed particles with homogenization treatment are denoted as homogenized 10 vol% and homogenized 20 vol% crushed refiners, respectively. To study the effect of $Al_{2.5}Cu_{0.5}Ti$ homogenization on the grain refining performance, an Al-10 vol% $Al_{2.5}Cu_{0.5}Ti$ refiner sample containing crushed particles without homogenization was also fabricated, and is denoted as unhomogenized 10 vol% crushed refiner. The notations used for the refiners are also shown in Fig. 2.

The microstructure, crystal structure, and composition of the prepared atomized particles, intermetallic compounds and fabricated refiners were investigated using optical microscopy (OM), scanning electron microscopy (SEM; JEOL JSM-5900LV), X-ray diffraction (XRD; Rigaku RINT-2100) with Cu-Kα radiation, and energy dispersive X-ray spectroscopy (EDS; JEOL JED-2200) analysis.

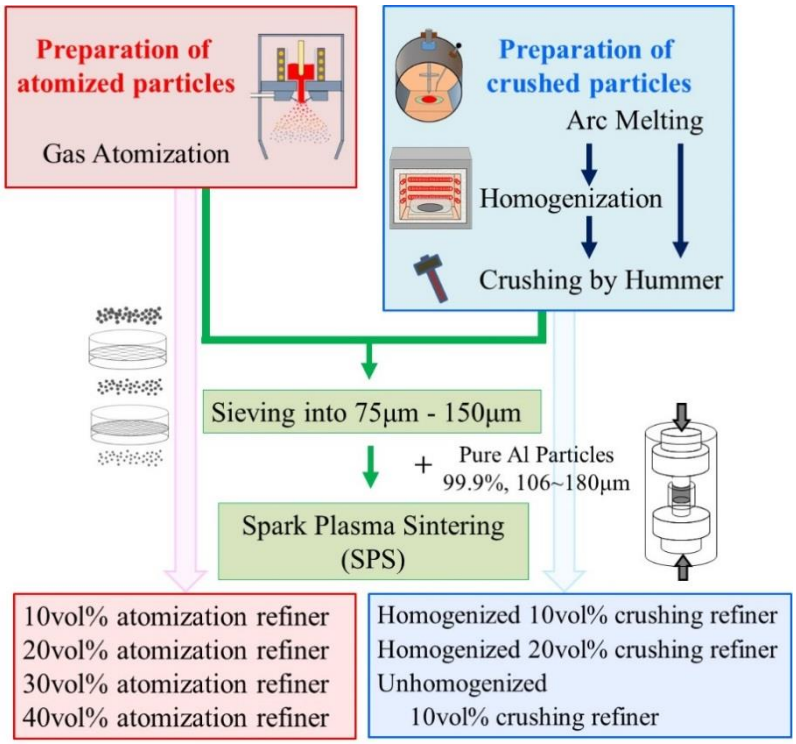


Fig. 2. Flow diagram for the fabrication of Al- $Al_{2.5}Cu_{0.5}Ti$ refiners.

### 2.2 Refining performance experiment

A commercially pure Al ingot (99.99%, 148.8 g for 10 vol% refiner, 149.4 g for 20 vol% refiner, 149.6 g for 30 vol% refiner, and 149.7 g for 40 vol% refiner) in an alumina crucible was melted in an electrical resistance furnace at 750 °C under an Ar atmosphere. The mass fractions of the Al–$Al_{2.5}Cu_{0.5}Ti$ refiners as additives were 0.8%, 0.4%, 0.27% and 0.2% for the 10, 20, 30, and 40 vol% refiners, respectively, so that the total amount of $Al_{2.5}Cu_{0.5}Ti$ particles within the melt was the same. After addition of the refiner into the melt, the melt was homogenized for 30 s by mechanical stirring and then held for a certain time (holding time) at 750 °C, and then poured into a steel mold (45 mm inner diameter, 70 mm outer diameter, 70 mm height). For grain size determination, each cast was cut horizontally at a distance of 5 mm from the bottom. The sectioned surface of the sample was polished and etched in 10% hydrofluoric acid aqueous solution, and the α-Al grains were observed. The mean size of α-Al grains was calculated using a mean linear intercept technique (Karlsson and Golhale (1997)).

## 3. Results and Discussion

### 3.1 Refining performance of atomization refiners

Figure 3 shows an SEM image of atomized $Al_{2.5}Cu_{0.5}Ti$ particles. The atomized particles appear to have almost spherical shape with some satellites on the surface. The compositions of the atomized particles in Fig. 3 were established using EDS and the composition results are given in Table 2. These compositions were thus confirmed to be close to the desired $Al_{2.5}Cu_{0.5}Ti$ intermetallic compound, *i.e.*, Al-12.5 mol% Cu-25 mol% Ti, except for the particle at point 4.

Figure 4 shows an XRD pattern for the atomized $Al_{2.5}Cu_{0.5}Ti$ particles. The (100) and (110) superlattice reflections of $Al_{2.5}Cu_{0.5}Ti$ phase with $L1_2$ structure are observed, which indicates an $L1_2$ structure. The lattice parameter of the atomized $Al_{2.5}Cu_{0.5}Ti$ particles with the $L1_2$ structure was calculated to be 0.3939 nm, which is in agreement with the reported value of 0.3927 nm (Villars and Calvert (1996)). However, a small unknown peak was also observed; therefore, the obtained atomized particles comprise the $L1_2$-modified $Al_{2.5}Cu_{0.5}Ti$ intermetallic compound, but contain a small amount of a secondary phase.

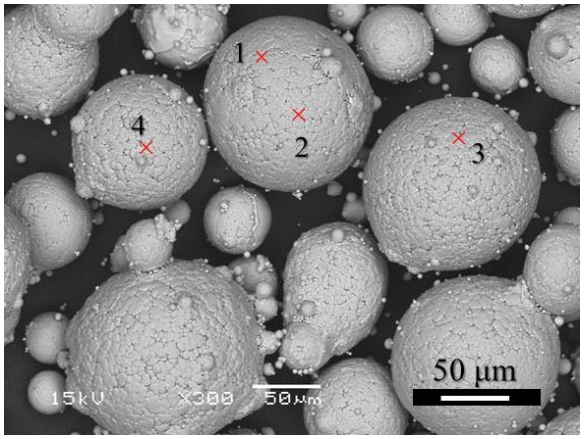

Fig. 3. SEM image of atomized $Al_{2.5}Cu_{0.5}Ti$ particles.

Table 2. Compositions of the obtained atomized particles labeled in Fig. 3 (mol%).

| | Al | Cu | Ti |
|---|---|---|---|
| $Al_{2.5}Cu_{0.5}Ti$ | 62.5 | 12.5 | 25.0 |
| 1 | 60.9 | 13.4 | 25.8 |
| 2 | 58.0 | 13.6 | 28.4 |
| 3 | 61.6 | 13.4 | 25.0 |
| 4 | 45.3 | 20.9 | 33.8 |

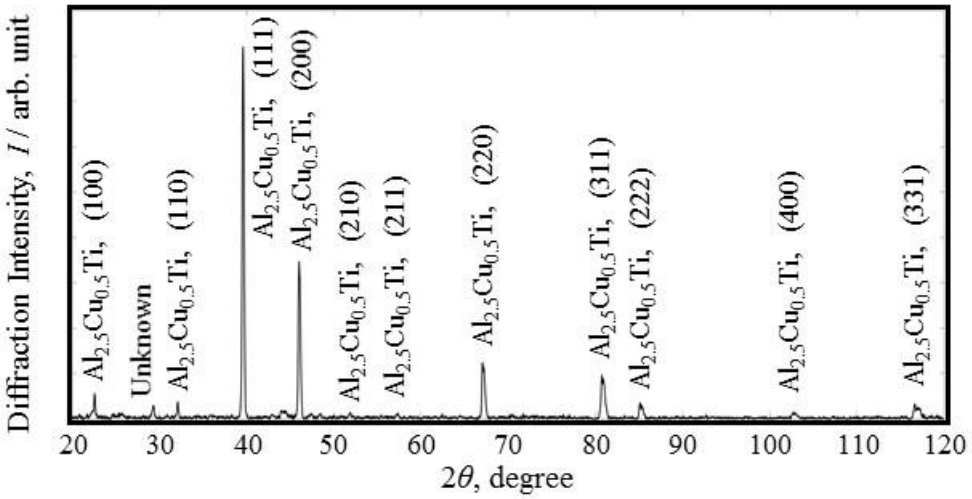


Fig. 4. XRD pattern for the atomized $Al_{2.5}Cu_{0.5}Ti$ particles.

SEM micrographs of the fabricated 10, 20, 30, and 40 vol% atomization refiners are shown in Figs. 5(a-d), respectively. Spherical shaped particles are homogeneously distributed in the Al matrix, even when there is a high volume fraction of refiner. The SPS process thus successfully produced fully dense refiners consisting of a high volume fraction of $Al_{2,5}Cu_{0.5}Ti$ particles embedded in the Al matrix. Figures 5(a'-d') show magnified SEM images of the 10, 20, 30, and 40 vol% atomization refiners, respectively. The chemical compositions at points 1 to 9 are listed in Table 3. The magnified SEM images show the atomized particles have a mesh shaped secondary phase without the stoichiometric composition of $Al_{2.5}Cu_{0.5}Ti$ (point 3 in Fig. 5 (a')). Moreover, reaction between the $Al_{2.5}Cu_{0.5}Ti$ intermetallic compound and the Al matrix was not evident at the interface, even though the refiners were fabricated by the sintering process.

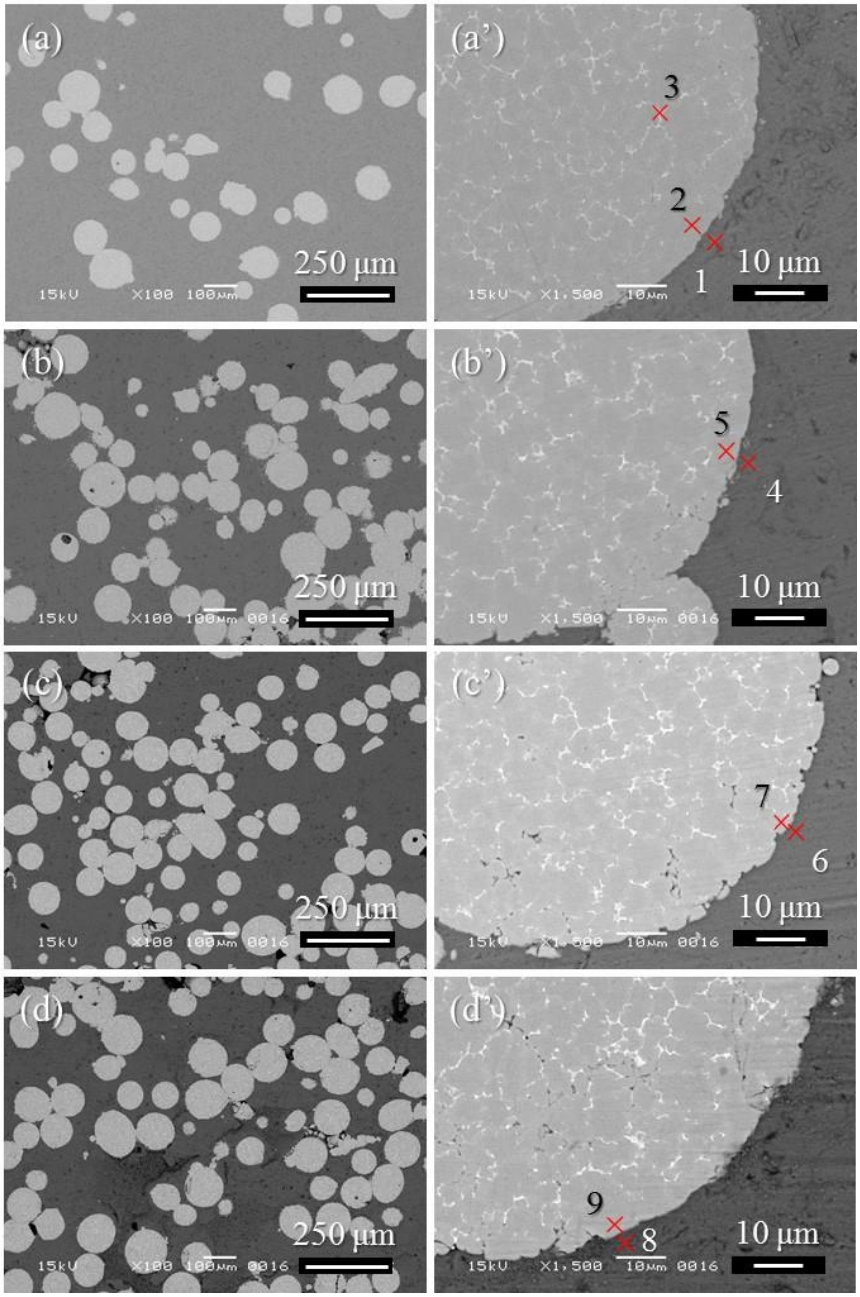


Fig. 5. SEM micrographs of fabricated (a,a') 10, (b,b') 20, (c,c') 30, and (d,d') 40 vol% atomization refiners.

Figures 6(a-d) show XRD patterns for the 10, 20, 30, and 40 vol% atomization refiners, respectively. Here, the (100) and (110) superlattice reflections of the $L1_2$ $Al_{2.5}Cu_{0.5}Ti$ phase were also observed. Considering the SEM observations (Fig. 5), the EDS results (Table 3) and the XRD patterns (Fig. 6), it is concluded that Al-$Al_{2.5}Cu_{0.5}Ti$ refiners with heterogeneous nucleation site particles with the $L1_2$ structure can be

successfully fabricated by the SPS method, even though the volume fraction of heterogeneous nucleation site particles in the refiners is high. The $Al_{2.5}Cu_{0.5}Ti$ intermetallic compound with the $L1_2$ structure has higher registry (lower *M* value) toward Al; therefore, it is expected that the fabricated Al-$Al_{2.5}Cu_{0.5}Ti$ refiners may exhibit better grain refining performance for Al cast alloys.

Table 3. EDS results for the obtained Al-$Al_{2.5}Cu_{0.5}Ti$ refiners at points labeled in Fig. 5 (mol%).

| | Al | Cu | Ti |
|---|---|---|---|
| $Al_{2.5}Cu_{0.5}Ti$ | 62.5 | 12.5 | 25.0 |
| 1 | 99.3 | 0.7 | 0.0 |
| 2 | 60.3 | 13.5 | 26.2 |
| 3 | 54.8 | 33.2 | 12.0 |
| 4 | 99.6 | 0.31 | 0.13 |
| 5 | 59.3 | 13.1 | 27.6 |
| 6 | 99.4 | 0.53 | 0.11 |
| 7 | 61.4 | 11.1 | 27.5 |
| 8 | 100.0 | 0.0 | 0.0 |
| 9 | 60.8 | 11.6 | 27.6 |

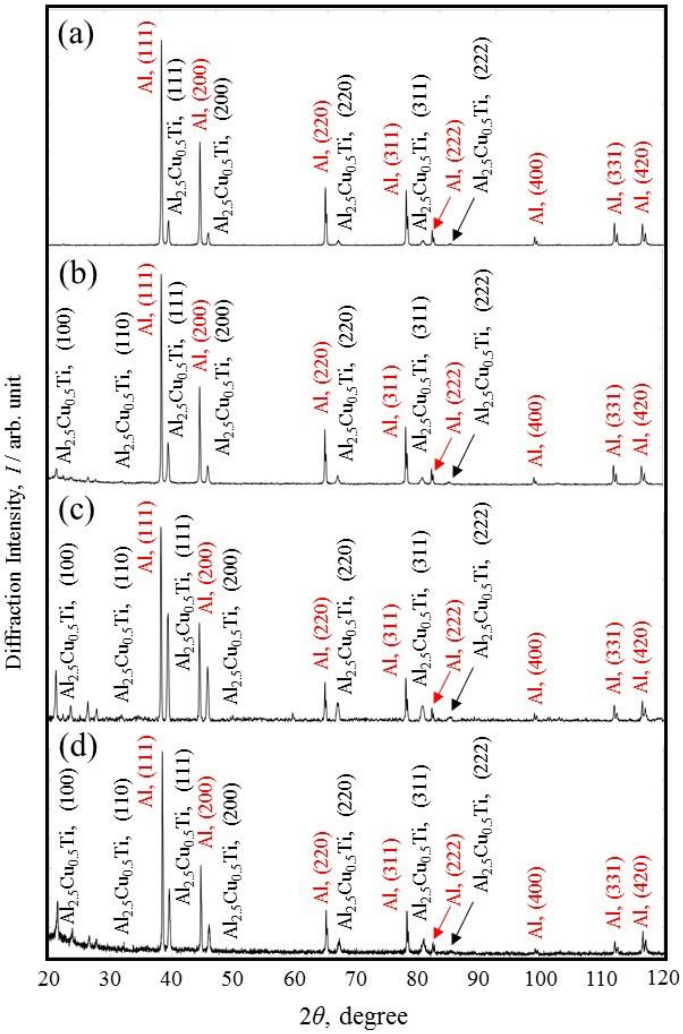


Fig. 6. XRD analyses of the fabricated (a) 10, (b) 20, (c) 30, and (d) 40 vol% atomization refiners.

The grain refining performance of the fabricated 10 vol% atomization refiner was tested by the addition of 1.2 g of the refiner into molten pure Al (148.8 g). Figure 7 shows a set of macrographs of Al casts with and without the 10 vol% atomization refiner. The Al cast without refiner shown in Fig. 7(a) has a coarse columnar grain structure with an average grain size of approximately 3908 μm. Figs. 7(b-f) show macrographs of Al casts prepared with holding times of 0, 180, 300, 360, and 600 s, respectively. Although equiaxed grains are observed at the outer regions, conversion of the coarse columnar grain structure to fine equiaxed grains occurs by the addition of the Al-10 vol% $Al_{2.5}Cu_{0.5}Ti$ refiner containing atomized particles, as shown in Figs. 7(b) to (f). In addition, fading of the grain refinement effect was noted at holding times longer than 360 s.

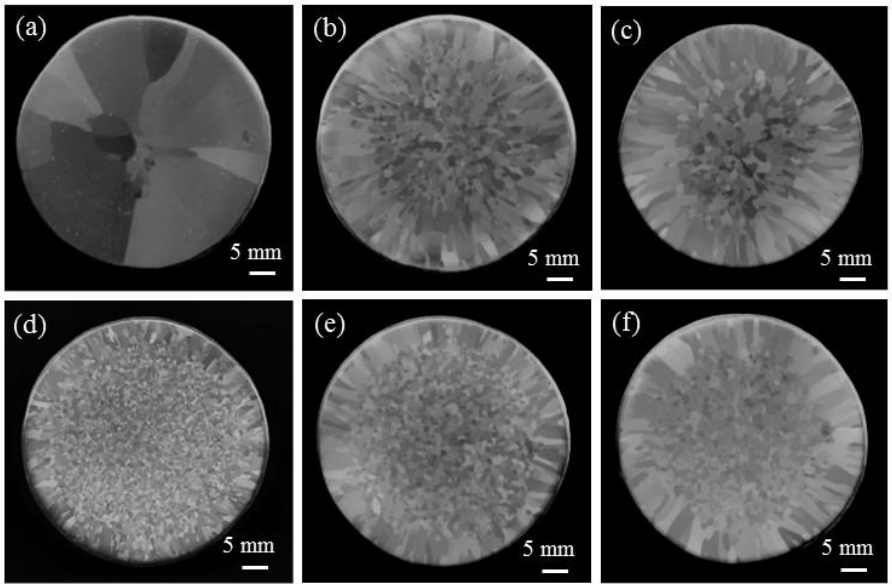


Fig. 7. Macrographs of Al casts, with and without the 10 vol% atomization refiner; (a) without refiner, and with refiner where the holding time was (b) 0, (c) 180, (d) 300, (e) 360 and (f) 600 s.

Figure 8 shows a set of macrographs of Al casts refined by 0.4% addition of the 20 vol% atomization refiner. The solidification structure of the Al casts refined with the 20 vol% atomization refiner became fine and equiaxed. The finest grain structure was observed in the Al cast prepared with a holding time of 420 s.

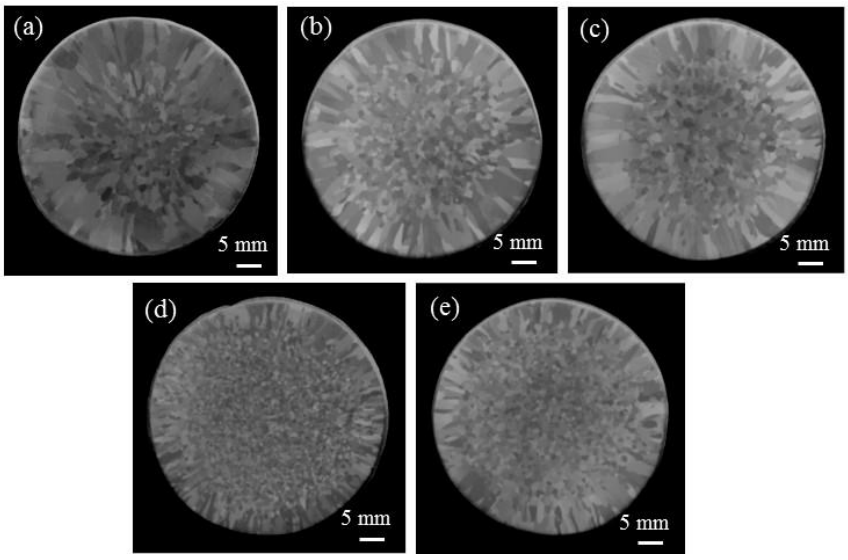


Fig. 8. Macrostructures of Al casts refined with the 20 vol% atomization refiner (0.4% addition) by hold times of (a) 0, (b) 180, (c) 300, (d) 420 and (e) 600 s.

The results of grain refinement performance tests for the 30 and 40 vol% atomization refiners at addition levels of 0.27% and 0.2% are shown in Figs. 9 and 10, respectively. Compared to the relatively good refinement performance of the 10 and 20 vol% atomization refiners for Al cast, lesser refinement performance was observed with the 30 and 40 vol% atomization refiners.

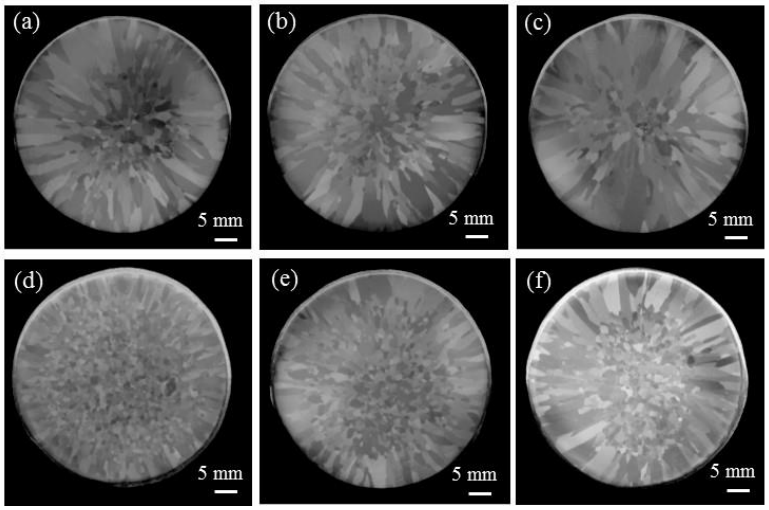


Fig. 9. Macrostructures of Al casts refined with the 30 vol% atomization refiner (0.27% addition) by hold times of (a) 0, (b) 300, (c) 420, (d) 540, (e) 600 and (f) 720 s.

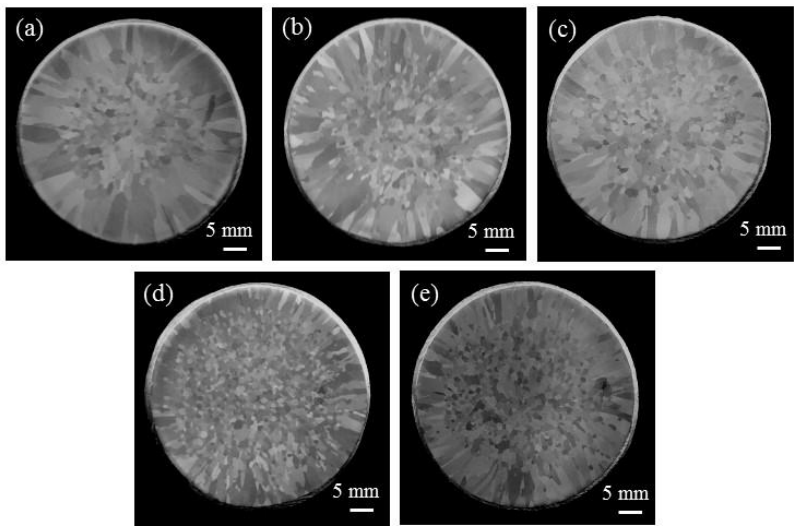


Fig. 10. Macrostructures of Al casts refined with the 40 vol% atomization refiner (0.2% addition) by hold times of (a) 0, (b) 420, (c) 540, (d) 600 and (e) 720 s.

Figure 11 shows the relation between the holding time and the average grain size of Al casts refined with the atomization refiners. The refiners containing different amounts

of heterogeneous nucleation site particles showed differences in the grain refining performance with the holding time, even though the total amount of $Al_{2.5}Cu_{0.5}Ti$ particles within the melt was the same. Grain refinement deteriorated as the volume fraction of heterogeneous nucleation site particles increased. The best holding times for the 10, 20, 30, and 40 vol% atomization refiners were determined to be 300, 420, 540, and 600 s, respectively. Longer holding time is required to achieve a uniform dispersion of $Al_{2.5}Cu_{0.5}Ti$ particles in the melt for the refiners with high volume fraction of heterogeneous nucleation site particles. In this way, fading of the grain refinement effect occurs slower when the volume fraction of heterogeneous nucleation site particles increased.

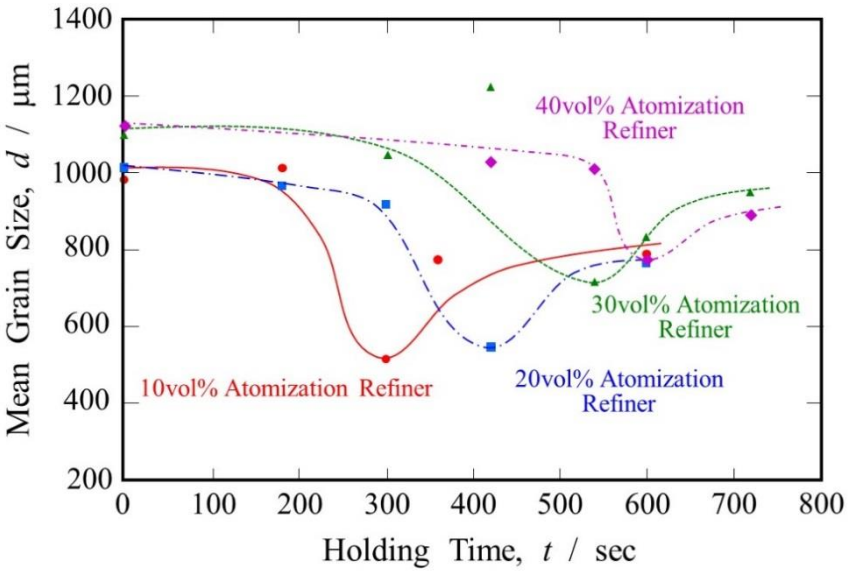


Fig. 11. Average grain size of Al casts refined with atomization refiners as a function of holding time at 750 °C. The levels of addition were 0.8%, 0.4%, 0.27% and 0.2% for the 0, 20, 30, and 40 vol% atomization refiners, respectively, so that the total amount of $Al_{2.5}Cu_{0.5}Ti$ particles within the melt was the same.

### 3.2 Refining performance of crushed refiners

Figures 12(a) and (b) show SEM micrographs for the $Al_{2.5}Cu_{0.5}Ti$ intermetallic compound sample prepared by arc melting before and after homogenization, respectively, and EDS analysis results are given in Table 4. Figure 12(a) shows that the untreated as-cast sample has a dual phase structure. The chemical composition of the matrix part of the untreated sample was determined to be Al-27.6 mol% Cu-11.3 mol% Ti, while the secondary phase was a Ti-poor and Cu-rich composition. In contrast, the treated sample

has a single phase structure, which indicates the secondary phase can be eliminated by homogenization at 1100 °C for 4 h. The chemical composition of the treated sample was Al-12.5 mol% Cu-27.4 mol% Ti. The stoichiometric composition of the $Al_{2.5}Cu_{0.5}Ti$ intermetallic phase is 62.5 mol% Al, 12.5 mol% Cu and 25 mol% Ti; therefore, the single phase $Al_{2.5}Cu_{0.5}Ti$ intermetallic compound with a stoichiometric composition can be obtained by arc melting and subsequent homogenization under these conditions. The bulk $Al_{2.5}Cu_{0.5}Ti$ intermetallic compound sample was crushed into fine particles with a hammer after the homogenization treatment, and the resultant particles are shown in Fig. 12(c). The homogenized crushed particles have granular shape and exhibit a fracture mode of brittle transgranular type cleavage (George et al. 1990).

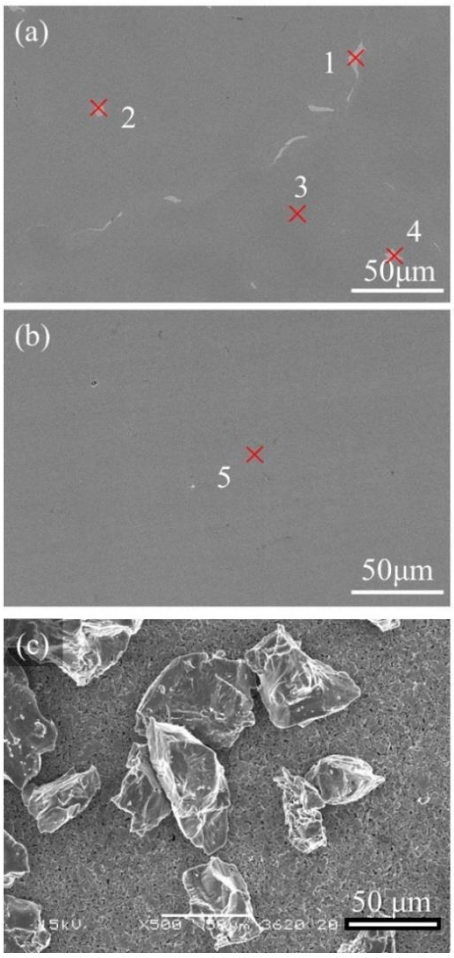


Fig. 12. SEM micrographs of $Al_{2.5}Cu_{0.5}Ti$ sample prepared by arc melting; (a) before homogenization treatment (as-cast), (b) after homogenization treatment, and (c) homogenized crushed $Al_{2.5}Cu_{0.5}Ti$ particles.

Table 4. Compositions of the sample prepared by arc melting at the points labeled in Fig. 12 (mol%).

| | Al | Cu | Ti |
|---|---|---|---|
| $Al_{2.5}Cu_{0.5}Ti$ | 62.5 | 12.5 | 25.0 |
| 1 | 44.4 | 54.5 | 1.1 |
| 2 | 44.8 | 54.1 | 1.13 |
| 3 | 61.1 | 11.3 | 27.6 |
| 4 | 56.9 | 28.4 | 14.7 |
| 5 | 60.2 | 12.5 | 27.4 |

Figures 13(a) and (b) show XRD patterns of the $Al_{2.5}Cu_{0.5}Ti$ samples before and after the homogenization, respectively. The (100) and (110) superlattice reflections of the $Al_{2.5}Cu_{0.5}Ti$ phase with the $L1_2$ structure were observed in both Figs. 13(a) and (b), which indicates that both samples have $L1_2$ structure. The lattice parameter of the $L1_2$ $Al_{2.5}Cu_{0.5}Ti$ phase in the samples was calculated to be 0.3917 nm, which is in agreement with the literature value of 0.3927 nm (Villars and Calvert (1996)).

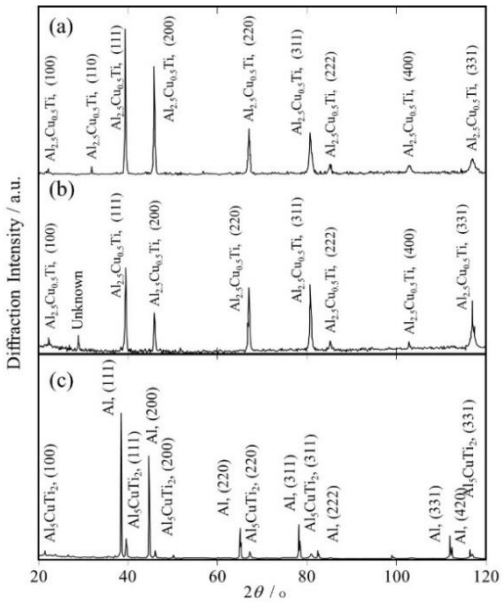


Fig. 13. XRD patterns for the $Al_{2.5}Cu_{0.5}Ti$ samples; (a) before and (b) after homogenization treatment. The lattice parameter of the $L1_2$ $Al_{2.5}Cu_{0.5}Ti$ phase in the sample was calculated to be 0.3917 nm. (c) XRD profile of homogenized 10 vol% crushed refiner.

To fabricate homogenized 10 vol% and 20 vol% crushed refiners, a mixed powder of the crushed intermetallic compound particles and pure Al particles was sintered

using the SPS apparatus at 500 °C for 5 min. Figure 13(c) shows the XRD pattern for the homogenized 10 vol% crushed refiner, which revealed only peaks that were consistent with phases of either A1 or the $Al_{2.5}Cu_{0.5}Ti$ intermetallic compound with the $L1_2$ structure.

Figures 14(a) and (b) show SEM micrographs of the homogenized 10 vol% and 20 vol% crushed refiners, respectively. These refiners have granular shaped particles homogeneously distributed within the Al matrix. Figures 14(a') and (b') show magnified SEM images of the homogenized 10 vol% and 20 vol% crushed refiners, respectively. The combination of XRD measurements (Fig. 13), SEM observations (Fig. 14) and the EDS results of particles shown in Table 5 indicate that the $L1_2$ type intermetallic compound particles successfully coexist with the Al matrix by the SPS process. The homogenized $Al_{2.5}Cu_{0.5}Ti$ intermetallic compound with the $L1_2$ structure has a smaller *M* value toward Al; therefore, it is expected that the homogenized crushed refiners may also exhibit better grain refining performance for Al cast alloys.

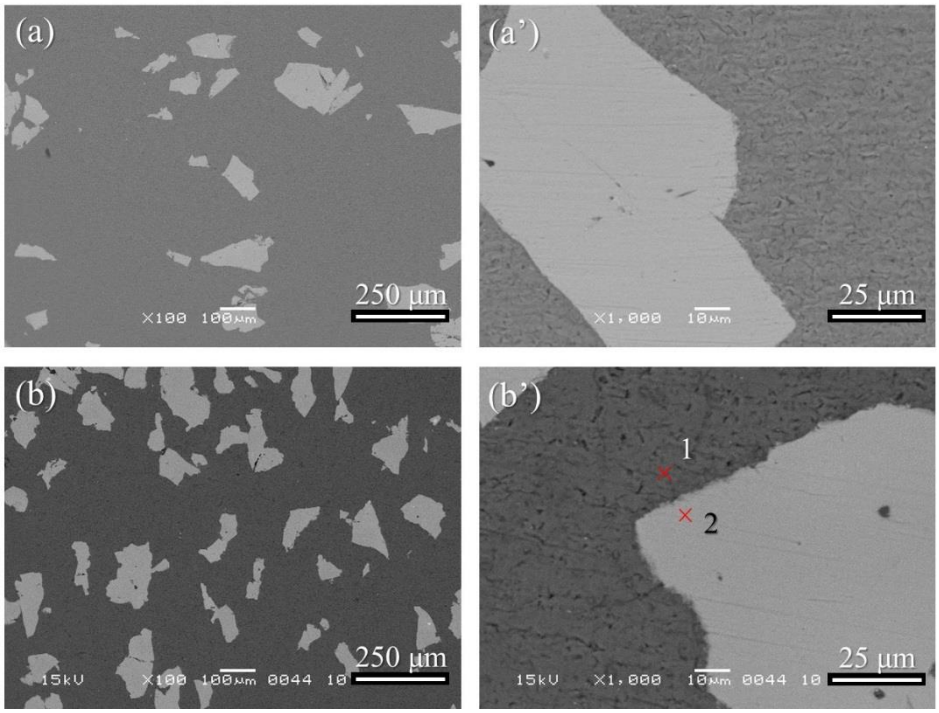


Fig. 14. SEM micrographs of (a,a') homogenized 10 vol% and (b,b') homogenized 20 vol% crushed refiners.

Table 5. EDS results of the homogenized 10 vol% crushed refiner for points labeled in Fig. 14 (mol%).

| | Al | Cu | Ti |
|---|---|---|---|

| | | | |
|---|---|---|---|
| $Al_{2.5}Cu_{0.5}Ti$ | 62.5 | 12.5 | 25.0 |
| 1 | 99.5 | 0.19 | 0.31 |
| 2 | 59.6 | 12.0 | 28.4 |

The grain refining performance of the homogenized 10 vol% and 20 vol% crushed refiners was tested, and the results are shown in Fig. 15. The grain size of the Al cast refined with the homogenized 10 vol% crushed refiner reached a minimum at 300 s and then has an ascending trend with the holding time, while the minimum grain size was obtained with the homogenized 20 vol% crushed refiner at 480 s. Therefore, the fading of the grain refinement effect is delayed by an increase in the volume fraction of heterogeneous nucleation site particles. Moreover, superior grain refining efficiency was obtained for the refiner containing crushed particles than with the refiner containing atomized particles shown in Fig. 11. The crushed particles have a single phase of the $Al_{2.5}Cu_{0.5}Ti$ intermetallic compound with the $L1_2$ structure after the homogenization treatment, while the atomized particles have a secondary phase, as shown in Fig. 6. The lattice matching between the nucleating substrate and the solid matrix is critical to the effectiveness of the substrate to refine a material by heterogeneous nucleation; therefore, it is considered that the secondary phase in $Al_{2.5}Cu_{0.5}Ti$ has a strongly negative effect on the grain-refining performance.

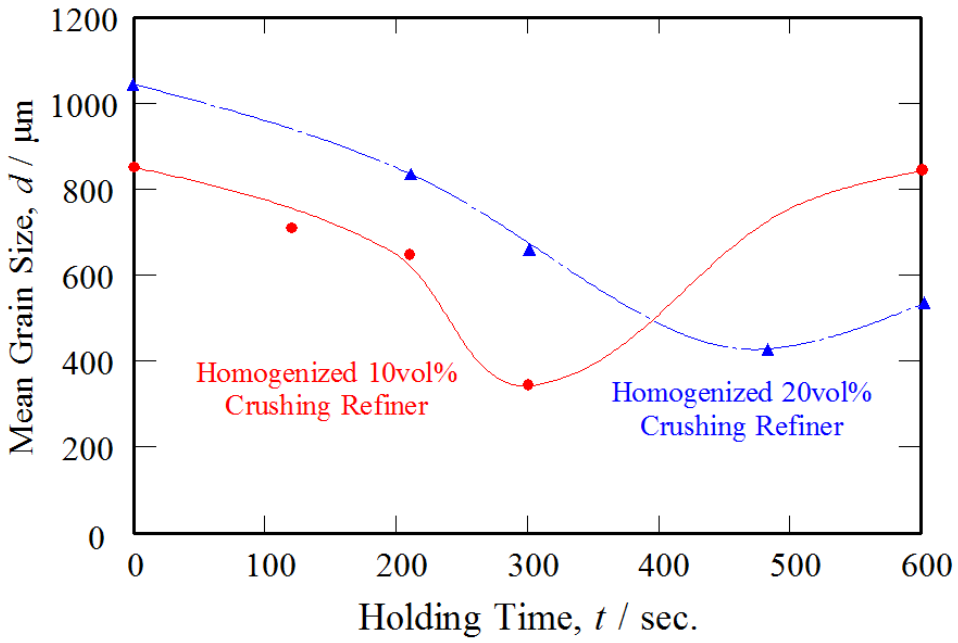


Fig. 15. Grain refining performance of the homogenized 10 vol% and 20 vol% crushed refiners as a function of the holding time at 750 °C.

Next, the influence of the secondary phase in the $Al_{2.5}Cu_{0.5}Ti$ refiner particles on the grain-refining efficiency was investigated. The unhomogenized 10 vol% crushed refiner with a certain amount of secondary phase was fabricated in the same manner. The average grain size of the Al casts refined with the unhomogenized 10 vol% crushed refiner is plotted as a function of the holding time in Fig. 16. The results for the homogenized 10 vol% crushed refiner and 10 vol% atomization refiner are also shown for comparison. Only a relatively small decrease in grain size is achieved by the unhomogenized 10 vol% crushed refiner. Different refining performance characteristics were apparent for refiners with different phases, even though the chemical compositions of the refiners themselves were the same. This is because the lattice matching between the heterogeneous nucleation site particles and solidified Al is critical to obtain finer grain structures for Al cast alloys.

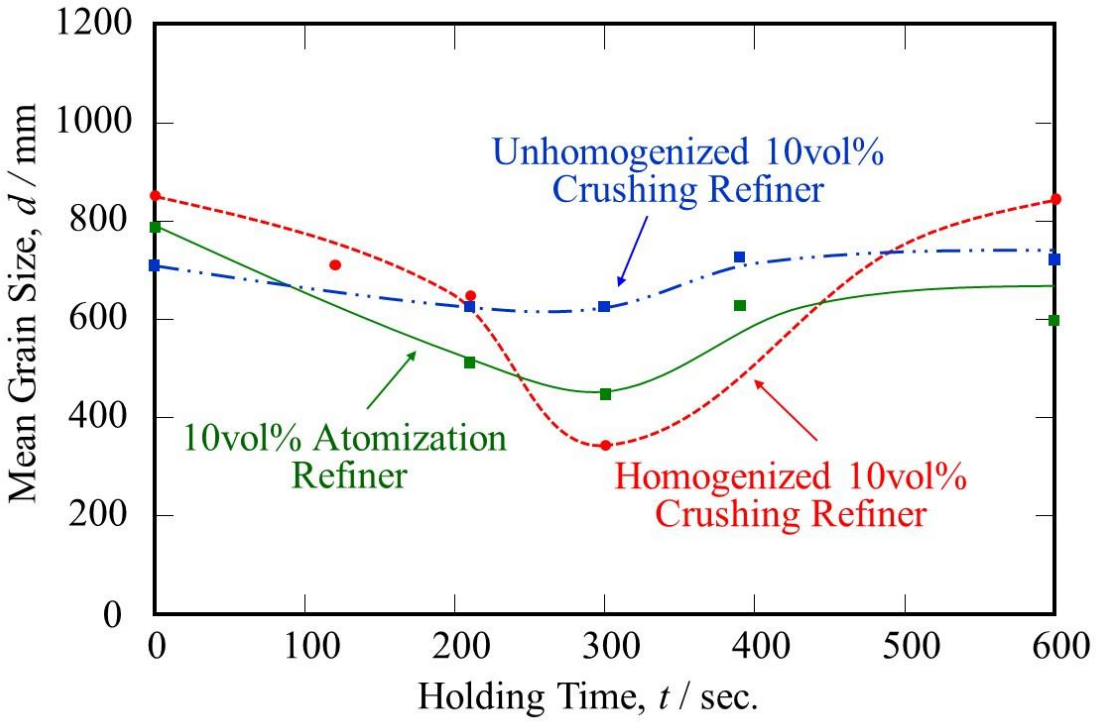


Fig. 16. Influence of the secondary phase in $Al_{2.5}Cu_{0.5}Ti$ refiner particles on the grain-refining efficiency as a function of the holding time at 750 °C.

## Conclusions

In this study, the grain refinement of Al casts using Al-$Al_{2.5}Cu_{0.5}Ti$ refiners with a high volume fraction of $L1_2$-modified heterogeneous nucleation site particles was investigated. Two types of $Al_{2.5}Cu_{0.5}Ti$ intermetallic compound particles with $L1_2$ structure were prepared, *i.e.*, crushed bulk material and that prepared by gas atomization. Al-$Al_{2.5}Cu_{0.5}Ti$ refiners were fabricated by the SPS method with volume fractions of $Al_{2.5}Cu_{0.5}Ti$ particles at 10, 20, 30 and 40 vol%. The grain refining performance of the fabricated refiners for pure Al casts was investigated and the following results were obtained.

1) Al-$Al_{2.5}Cu_{0.5}Ti$ refiners containing $L1_2$-modified heterogeneous nucleation site particles can be successfully fabricated by the SPS method, even though the volume fraction of $Al_{2.5}Cu_{0.5}Ti$ particles is high.
2) Fabricated Al-$Al_{2.5}Cu_{0.5}Ti$ refiners were effective grain refiners for pure Al because $Al_{2.5}Cu_{0.5}Ti$ particles with the $L1_2$ structure acts as nuclei for Al grains in Al melts. The fading of the grain refinement effect occurs slower when the volume fraction of heterogeneous nucleation site particles increased.
3) Different refining performance characteristics appeared for refiners with different phases, even though the chemical compositions of the refiners themselves were the same. This is because the lattice matching between heterogeneous nucleation site particles and solidified Al is critical to obtain finer grain structures for Al casts.
4) Finer grained Al casts can be obtained using heterogeneous nucleation sites with higher lattice matching between heterogeneous nucleation site particles and solidified Al.

*Acknowledgements*

This work was funded through a project subsidized by the New Energy and Industrial Technology Development Organization (NEDO). Part of this research was also supported by the Japan Science and Technology Agency (JST) under the Industry-Academia Collaborative R&D Program "Heterogeneous Structure Control: Towards Innovative Development of Metallic Structural Materials". Two of the authors (YW and HS) would also like to thank The Light Metal Educational Foundation Inc. of Japan for financial support.

## References

Bramfitt, B.L., 1970. The effect of carbide and nitride additions on the heterogeneous

nucleation behavior of liquid iron. Metall. Trans. A 1, 1987-1995.
Fan, Z., Wang, Y., Zhang, Y., Qin, T., Zhou, X.R., Thompson, G.E., Pennycook, T., Hashimoto, T., 2015. Grain refining mechanism in the Al/Al–Ti–B system. Acta Mater. 84, 292-304.
George, E.P., Horton, J.A., Porter, W.D., Schneibel, J.H., 1990. Brittle cleavage of $L1_2$ trialuminides. J. Mater. Res. 5, 1639-1648.
GunnÆs, A.E., Olsen, A., Taftφ, J., 1998. Microstructure development in laser-processed Al–Ti–Ni Alloys with 25 at.% Ti. J. Mater. Sci. 20, 4961-4969.
Honda, K., Ushioda, K., Yamada, W., Tanaka, K., Hatanaka, H., 2008. Nucleation of the primary Al phase on $TiAl_3$ during solidification in hot-dip Zn-11%Al-3%Mg-0.2%Si - coated steel sheet, Mater. Trans. 49, 1401-1409.
Inoue, H.R.P., Cooper, C.V., Favrow, L.H., Hamada, Y., Wayman, C.M., 1991. Mechanical properties of Fe-modified $Ll_2$-Type $Al_3Ti$, MRS Proceedings 213, 493-498.
Karlsson, L.M., Golhale, A.M., 1997. Stereological estimation of mean linear intercept length using the vertical sections and trisector methods. J. Microscopy 186, 143-152.
Kato, M., Wada, M., Sato, A., Mori, T., 1989. Epitaxy of cubic crystals on (001) cubic substrates. Acta Metal. 37, 749-756.
Mabuchi, H., Nakayama, Y., 1991. Development of Al-Ti-X ternary $L1_2$ intermetallic compounds, Bull. Jpn Inst. Metals 30, 24-30 (in Japanese).
Mazdiyasni, S., Miracle, D.B., Dimiduk, D.M., Mendiratta, M.G., Subramanian, P.R., 1989. High temperature phase equilibria of the $Ll_2$ composition in the Al-Ti-Ni, Al-Ti-Fe, and Al-Ti-Cu systems. Scripta Metall. 23, 327-331.
Nakayama, Y., Mabuchi, H., 1993. Formation of ternary $L1_2$ compounds in $Al_3Ti$-base alloys. Intermetallics 1, 41-48.
Sato, H., Ota, K., Kato, H., Furukawa, M., Azuma, M., Watanabe, Y., Zhang, Z., Tsuzaki, K., 2013. Grain refinement of as-cast pure Al by cold-rolled Al-Ti alloy refiner. Mater. Trans. 54, 1554-1561.
Turnbull, D., Vonnegut, B., 1952. Nucleation catalysis. Ind. Eng. Chem. 44, 1292-1298.
Venkateswarlu, K., Murty, B.S., Chakraborty, M., 2001. Effect of hot rolling and heat treatment of Al–5Ti–1B master, Mater. Sci. Eng. A301, 180-186.
alloy on the grain refining efficiency of aluminium
Villars, P., Calvert, L.D., 1996. Pearson's Handbook of Crystallographic Date for Intermetallic Phases (ASM International, Materials Park, OH), p. 958, p. 981, p. 1043.
Watanabe, Y., Eryu, H., Matsuura, K., 2001. Evaluation of three-dimensional orientation of $Al_3Ti$ platelet in Al based FGMs fabricated by a centrifugal casting technique, Acta Mater. 49, 775-783.

Watanabe, Y., Hamada, T., Sato, H., 2016. Fabrication of novel Al–$L1_2$-type $Al_{2.7}Fe_{0.3}Ti$ refiners by spark plasma sintering and their refining performance. Jpn. J. Appl. Phys. 55, 01AG01 (10 pages).
Watanabe, Y., Zhou, Q., Sato, H., Fujii, T., Inamura, T., 2017a. Microstructure of Al-$Al_3Ti$ functionally graded materials fabricated by centrifugal solid-particle method and centrifugal in situ method. Jpn J. Appl. Phys. 56, 01AG01 (11 pages).
Watanabe, Y., Hamada, T., Sato, H., 2017b. Decomposition of $Al_{2.7}Fe_{0.3}Ti$ in heated Al-$Al_{2.7}Fe_{0.3}Ti$ refiner fabricated by spark plasma sintering and its refining performance. Jpn J. Appl. Phys. 56, 01AG02 (7 pages).
Yamashita, K., Watanabe, C., Kumai, S., Kato, M., Sato, A., Watanabe, Y., 2000. Cyclic deformation and development of dislocation structures in a centrifugally cast Al-$Al_3Ti$ of functionally graded material. Mater. Trans., JIM 41, 1322-1328.
Zhang, Z., Watanabe, Y., Kim, I. S., Liu, X., Bian, X., 2005a. Microstructure and refining performance of an Al-5Ti-0.25C refiner before and after equal-channel angular pressing. Metall. Mater. Trans. A 36, 837-844.
Zhang, M.-X., Kelly, P.M., Easton, M.A., Taylor, J.A., 2005b. Crystallographic study of grain refinement in aluminum alloys using the edge-to-edge matching model. Acta Mater. 53, 1427-1438.
Zhang, Z., Shen, X., Zhang, C., Wei, S., Lee, S., Wang, F., 2013. A new rapid route to in-situ synthesize TiB-Ti system functionally graded materials using spark plasma sintering method. Mater. Sci. Eng. A 565, 326-332.

Figure captions

Fig. 1. Al-rich corner of the Al-*Me*-Ti (*Me* = Ni, Fe and Cu) alloy diagram at 1200 °C showing $L1_2$ regions, after Mazdiyasni et al. (1989). Schematic illustrations of $Al_3Ti$ with the $D0_{22}$ structure, Al with an fcc structure and $(Al_{1-x}Me_x)_3Ti$ with the $L1_2$ structure, as well as their lattice parameters, after Villars and Calvert (1996).
Fig. 2. Flow diagram for the fabrication of Al- $Al_{2.5}Cu_{0.5}Ti$ refiners.
Fig. 3. SEM image of atomized $Al_{2.5}Cu_{0.5}Ti$ particles.
Fig. 4. XRD pattern for the atomized $Al_{2.5}Cu_{0.5}Ti$ particles.
Fig. 5. SEM micrographs of fabricated (a,a') 10, (b,b') 20, (c,c') 30, and (d,d') 40 vol% atomization refiners.
Fig. 6. XRD analyses of the fabricated (a) 10, (b) 20, (c) 30, and (d) 40 vol% atomization refiners.
Fig. 7. Macrographs of Al casts, with and without the 10 vol% atomization refiner; (a)

without refiner, and with refiner where the holding time was (b) 0, (c) 180, (d) 300, (e) 360 and (f) 600 s.

Fig. 8. Macrostructures of Al casts refined with the 20 vol% atomization refiner (0.4% addition) by hold times of (a) 0, (b) 180, (c) 300, (d) 420 and (e) 600 s.

Fig. 9. Macrostructures of Al casts refined with the 30 vol% atomization refiner (0.27% addition) by hold times of (a) 0, (b) 300, (c) 420, (d) 540, (e) 600 and (f) 720 s.

Fig. 10. Macrostructures of Al casts refined with the 40 vol% atomization refiner (0.2% addition) by hold times of (a) 0, (b) 420, (c) 540, (d) 600 and (e) 720 s.

Fig. 11 Average grain size of Al casts refined with atomization refiners as a function of holding time at 750 °C. The levels of addition were 0.8%, 0.4%, 0.27% and 0.2% for the 0, 20, 30, and 40 vol% atomization refiners, respectively, so that the total amount of $Al_{2.5}Cu_{0.5}Ti$ particles within the melt was the same.

Fig. 12. SEM micrographs of $Al_{2.5}Cu_{0.5}Ti$ sample prepared by arc melting; (a) before homogenization treatment (as-cast), (b) after homogenization treatment, and (c) homogenized crushed $Al_{2.5}Cu_{0.5}Ti$ particles.

Fig. 13. XRD patterns for the $Al_{2.5}Cu_{0.5}Ti$ samples; (a) before and (b) after homogenization treatment. The lattice parameter of the $L1_2$ $Al_{2.5}Cu_{0.5}Ti$ phase in the sample was calculated to be 0.3917 nm. (c) XRD profile of homogenized 10 vol% crushed refiner.

Fig. 14. SEM micrographs of (a,a') homogenized 10 vol% and (b,b') homogenized 20 vol% crushed refiners.

Fig. 15. Grain refining performance of the homogenized 10 vol% and 20 vol% crushed refiners as a function of the holding time at 750 °C.

Fig. 16. Influence of the secondary phase in $Al_{2.5}Cu_{0.5}Ti$ refiner particles on the grain-refining efficiency as a function of the holding time at 750 °C.

Table captions

Table 1. *M* values between Al and $Al_3Ti$, $TiB_2$ or $Al_{2.5}Cu_{0.5}Ti$.

Table 2. Compositions of the obtained atomized particles labeled in Fig. 3 (mol%).

Table 3. EDS results for the obtained Al-$Al_{2.5}Cu_{0.5}Ti$ refiners at points labeled in Fig. 5 (mol%).

Table 4. Compositions of the sample prepared by arc melting at the points labeled in Fig. 12 (mol%).

Table 5. EDS results of the homogenized 10 vol% crushed refiner for points labeled in Fig. 14 (mol%).